1. Nucleosynthetic Yields From Various Sources

In this section we discuss the various sites for producing the heavy elements, and give a guide to the literature and to sources for the yields for each process. Talbot & Arnett (1973, ApJ, 186, 69) defined a stellar production matrix, which describes the production of each isotope in a star of initial mass m. One element of this matrix, $Q_{ij}(m)$, represents the fraction of the stellar mass which was originally present in the form of species j and is eventually ejected by the star in the form of element i, so $Q_{ij}(m) = (m_{ej})_{ij}(m)/(mX_j)$, where X_j is the abundance by mass of element j already present in the star when it first formed.

Then the total contribution of a star of mass M to the ejected mass of the element i, both newly formed, and originally present, is given by

$$(M_{ej})_i \;=\; \sum_{j=1,n} Q_{ij}(M)\; X_j\; M.$$

In most modern calculations, the yield for element i is given without the detail of what was the initial form of i before nucleosynthesis, i.e. the production yield $p_{im} = (M_{ej})_i/M$. The dependence on j is treated by carrying out the calculation of yields for various stellar metallicities at each stellar mass.

Galactic yields y_i are then the sum over a stellar generation with a specific IMF, taking into account the minimum mass that dies (usually set to $1M_\odot$) and the remnants (white dwarfs, neutron stars, black holes) for each species i.

Remember that the mass of a highly evolved star is its initial mass − mass lost during evolution through winds. This early lost material has a chemical inventory close to or identical to that of the star when it was formed. Then there is the mass ejected near the end of the star's lifetime (during the supernova, nova, etc), which will contain highly

processed material from the stellar interior as well as the outer layers of the star. Thus to calculate the yields you need a detailed understanding of the last stages of stellar evolution, of the explosion that might occur, and of the mass cutoff for ejection, as well as the nuclear reaction network itself.

1.1. The Neutron Excess

Naively one might think that the nuclear reaction rates depend only on T, ρ, and the initial chemical composition. But there is another important parameter, related to the intitial chemical composition, the neutron excess.

Neutrons and protons can interconvert via weak interactions, and these conversions occur during decays. The second reaction listed below, when only the right arrow holds, is electron capture, while the third is β-decay.

$$p + \overline{\nu} \rightleftharpoons n + e^+, \quad p + e^- \rightleftharpoons n + \nu, \quad n \rightleftharpoons p + e^- + \overline{\nu}.$$

Free neutrons decay with a mean lifetime of $\sim$15 min via the last of the three reactions listed above.

Depending on whether there is enough time for the various unstable isotopes that may be produced to decay, one can end up with different isotopic compositions. This is not only the case for the neutron capture processes, but also for nuclear reactions in explosions, where the timescale may be so short that β-decays cannot happen. In addition, the formation of neutron-rich isotopes, be they stable or unstable, is more rapid if there are excess neutrons.

We must have a constant total number of nucleons. If weak interactions (decays)

cannot occur fast enough, we will have a constant number of protons and a constant number of neutrons, $N_n + N_p = \sum_i N_i A_i$, where A_i is the atomic mass of the isotope and the sum is over all isotopes i present.

The neutron excess per nucleon, η, is $(N_n - N_p)/(N_n + N_p)$. By charge neutrality, the electron number is the total number of protons, and, since the material is fully ionized, $Y_e = \sum_i Y_i Z_i$, where Y_e is the fraction of electrons in a fixed mass of the plasma and Z_i is the charge of each isotope i. By definition, $\sum_i Y_i A_i = 1$, so one can show that $\eta = 1 - 2Y_e$. Thus the neutron excess is related to a deficit of free electrons in the plasma.

Consider He burning in a convective core at $T \sim 10^8$ K. ^{18}O, with 8 protones and 10 neutrons, can be produced by $^{14}\mathrm{N}(\alpha,\gamma)^{18}\mathrm{F}$, followed by decay of ^{18}F to ^{18}O. This is important because it converts a relatively abundant nucleus with no neutron excess (^{14}N) into a nucleus with a neutron excess of $(2/18) = 0.111$. For solar abundances, at this stage of stellar evolution and nuclear processing in the core, this gives a total neutron excess of $\eta \approx 1.5 \times 10^{-3}$.

Primordial gas is mostly H, which has only one proton, and no neutrons, and hence the initial neutron excess is negative. As H burning proceeds, H is converted into ^{4}He and ^{12}C, both of which have a neutron excess of 0. Then, after He burning, η becomes slightly positive as a small neutron excess builds up through production of ^{18}O.

Since decays cannot happen during explosive nucleosynthesis (i.e. in modeling SNII), the input neutron excess is identical to that of the final burned products that are eventually ejected. Using the value $\eta = 1.5 \times 10^{-3}$ in explosive nucleosynthesis calculations reproduces the ratios of neutron-rich nuclei to their neighbors in the periodic table for the solar composition. If a value significantly different is chosen, the predicted final isotopic ratios do not match those for the Sun.

2. SNIa

SNIa are usually believed to be explosions of white dwarfs that have approached the Chandrasekhar limit ($M_{ch} \sim 1.39 M_{\odot}$) through accretion from a companion in a binary system, although in his recent colloquium Martin van Kerkwijk suggested a somewhat different mechanism, the merging of two C-O white dwarfs. The white dwarfs are disrupted by thermonuclear fusion of C and O from accreted material heated up by packing even more accreted material on top of the white dwarf. Thus the details depend on the accretion rate from the companion, among other parameters. Given these issues, SNIa yields are very hard to calculate.

SNIa are used as standard candles in cosmology, and it therefore behooves us to understand the explosion mechanism, and the resulting nucleosynthesis, well.

SNIa contribute very significantly to the Fe-peak elements. Their production of lighter element is considerably less important. They produce very little of elements lighter than Al. The first yield calculations were by Iwamoto, Brachwitz, Nomoto et al (1999, ApJS, 125, 439). Recently Travaglio, Hillebrandt, Reinecke & Thielemann (2004, A&A, 425, 1029) present 2D and 3D hydrodynamical models of SNIa and a new set of nucleosynthesis yields.

The latest calculations of SNIa detonations are given by Woosley, Kerstein, Sankaran & Ropke (2009, ApJ, 704, 255). These are deflagrations, a flame front of combustion propagating at subsonic speeds through the transfer of heat, which may turn into detonations (the same propagating at supersonic speeds). These flame fronts have a lot of instabilities, making the calculations very difficult. They note that the Reynolds number in a SNIa is orders of magnitude greater than any achieved in a terrestrial experiment or numerical simulation due to the viscosity of electron-ion interactions in a fully ionized dense plasma.

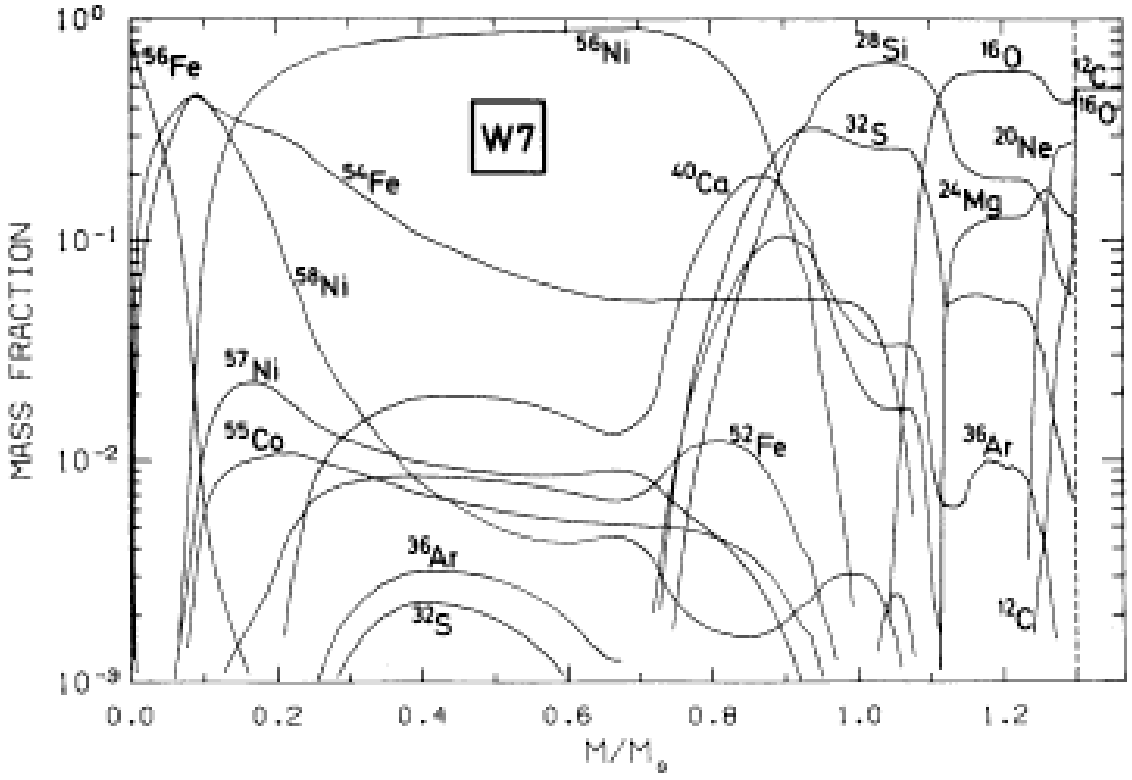

Fig. 1.— Mass fraction of a few major nuclei resulting from C-deflagration prediced by Nomoto (Fig. 7a from Nomoto (1984, ApJ, 286, 644).

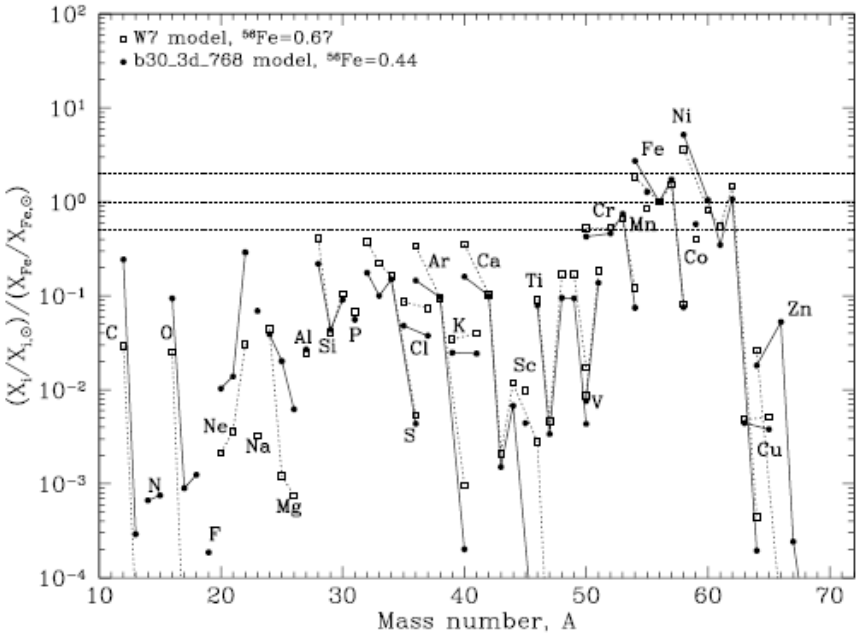

Fig. 9. Nucleosynthetic yields (in mass fraction normalized to the solar value and to the corresponding solar ratio) obtained using 19683 tracer particles in the 3D model *b30_3d_768* compared to the W7 yields given by Thielemann et al. (2003).

Fig. 2.— Fig. 9 from Travaglio et al (2004). The light elements are depleted relative to the Solar mixture while the Fe-peak elements are strongly produced.

3. Core Collapse SN Yields

Core collapse SN are the end phase of evolution of massive stars in the range of 8 to $\sim$130$M_{\odot}$. A single SN in the early galaxy can substantially enrich all the gas in the halo, so understanding their yields is quite important. The yields depend on the mass of the progenitor, the amount of mass loss during normal stellar evolution, the explosion energy, the mass cutoff (mass above the cutoff is ejected, that below settles into the remnant, a black hole), mixing around the cutoff area, and the mass of ^{56}Ni produced. Since it is so difficult to model SN, with so much poorly understood physics, that noone can make one explode in a computer, these calculations are tuned by matching the characteristics of observed SN, including of course SN1987A in the LMC. From the observed light curve and spectral fitting of individual SN, the explosion energy and produced ^{56}Ni mass can be determined.

Unlike SNIa, the core collapse family of SN is very diverse in their characteristics, luminosity, spectra (some show hydrogen lines, others no H, but strong He, others neither H nor He, presumably depending on the amount of mass lost prior to the explosion), explosion energy, etc. Most models are spherically symmetric, but that may not match reality.

Currently three varieties are recognized: very energetic hypernovae, with kinetic energy about 10 times larger than normal SNII, i.e. $> 10^{52}$ ergs, which probably form black holes as remnants, normal core collapse SN with explosion energy $\sim 10^{51}$ ergs, and very faint and low energy SN, which may be characterized by a lot of fall-back so that most of the Fe ends up in the black hole rather than being ejected. Their progenitors were probably at the low end of the mass of the core-collapse SN family.

In addition to enriching the ISM, these energetic events have strong dynamical and thermal influences on the ISM, discussed in the section on feedback. The relationship of core-collapse SN to GRBs is another area of great current interest.

Two burning regions, incomplete and complete Si-burning, dominate the nucleosynthesis production. The latter, at $T_{peak} > 5 \times 10^9$ K, produces large amounts of Co, Zn, V, and Cr; the former produces Cr and Mn. Both produce ^{56}Ni, which eventually becomes ^{56}Fe. The details depends on the neutron excess, which in turn depends on the metallicity, and in particular affects the production of the odd atomic number Fe-peak elements, i.e. Mn and Co, hence the odd-even effect. A high explosion energy enhances the α-rich freezeout (see the section in the notes on nuclear reaction rates regarding late stages of evolution in massive stars), hence the production of Zn and Co.

Several groups calculate yields for these SN. One is led by Ken Nomoto in Japan and another by Stan Woosley at UC Santa Cruz. The first major set of calculations was by Woosley & Weaver (1995, ApJS, 101, 181), while some of their latest yields are given in Heger & Woosley (2009, ApJ, see arXiv:0803.3161).

Nomoto, Tominaga, Umeda, Koayashi & Maeda (2006, Jrl. Nuc. Phys. A777, 424) is a good summary of the work of the Japanese group. Table 2 of their paper give the detailed yields (mass in units of the Solar mass) in the ejecta for each isotope a function of inital stellar mass and metallicity. Table 3 gives the IMF weighted yields as well.

The Italian Group have also published yields for core collapse SN, see their latest set given in Chieffi & Limongi (2004, ApJ, 608, 405). Note that no elements above Zn are produced by any mass in their grid up to a metallicity of $\sim 10^{-3}$ that of the Sun. That is true of calculations by other groups as well.

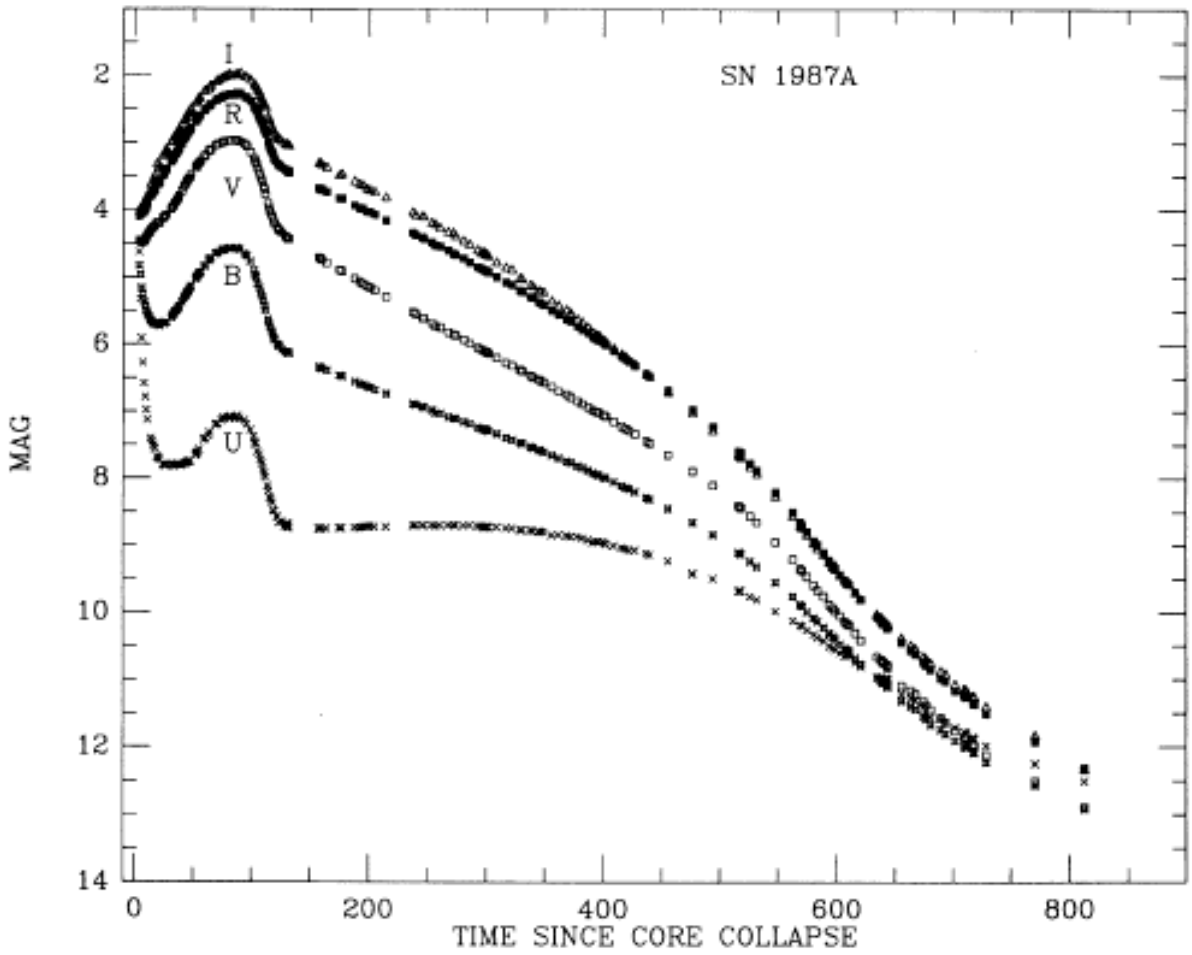

Fig. 3.— Fig. 1 from Hamuy & Suntzeff, 1990 (AJ). Light curves in various optical bandpasses for SN 1987A in the LMC.

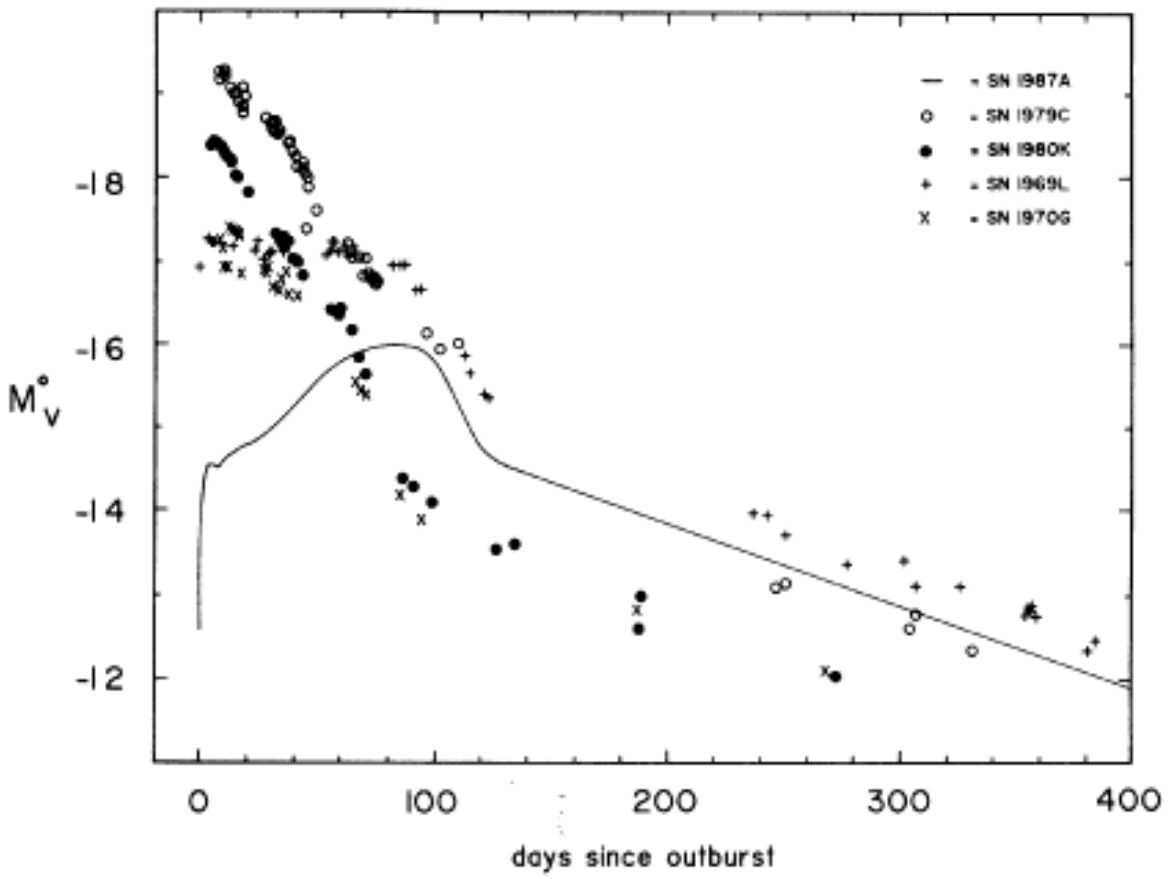

Fig. 4.— Fig. 5 from Hamuy & Suntzeff, 1990 (AJ, 99, 1146). Light curves of the absolute visual magnitude for a number of SNII with data extending to more than 100 days, including SN 1987A. Note that from day 130 to 400, all the SNII fall with roughly the same exponential rate of decline. Compared to the very large variation in intrinsic brightness near the peak and during the first 100 days, the absolute V mags of the SNII after day 130 are remarkably similar.

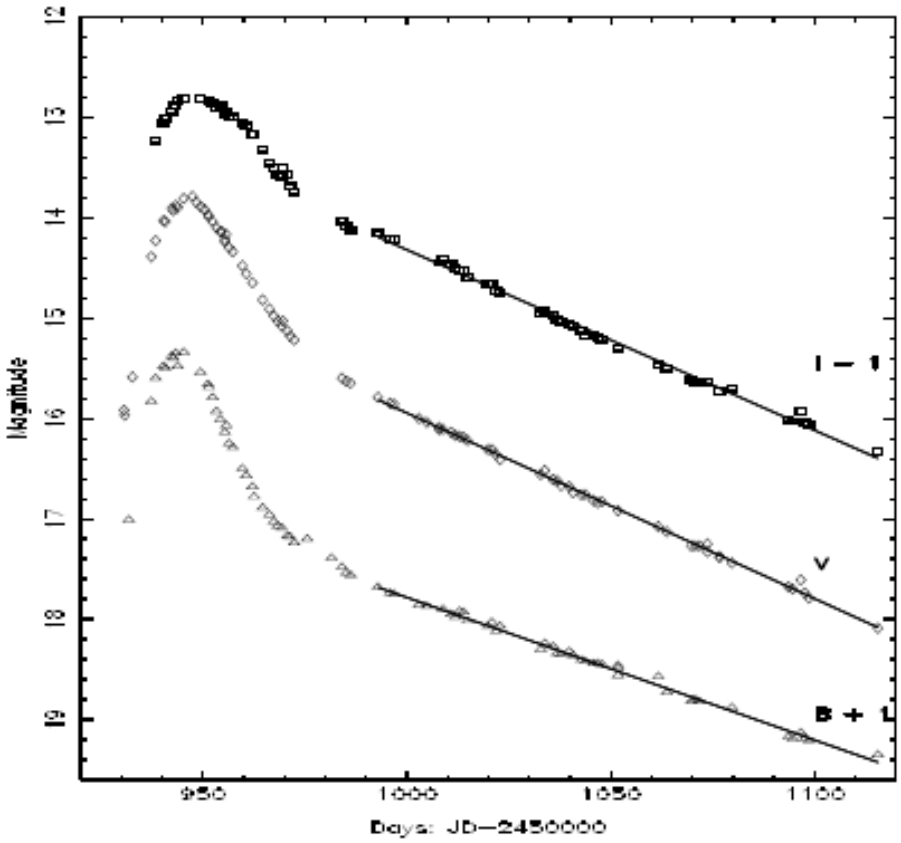

Fig. 1.— B, V, and I light curves for SN 1988bw. Galama et al. (1998) data are all from before day 986 (JD2450986) while ours begin on day 992 (JD2450992). The best fit lines show a remarkably good fit to our measured late time observations with no significant deviations at any time or in any color. The corresponding decay half-lives are 53.4 ± 0.8, 40.9 ± 0.7, and 41.6 ± 0.7 days in B, V, and I respectively. The closeness of the magnitude-versus-time relation to a line and the similarity of the decline rates with those for Type Ia supernovae are suggestive that the decay of radioactive cobalt might be the source powering the tail with leakage of gamma radiation. The overall light curve shape is similar to those of Type Ia, Ib, Ic and IIL supernovae. Our measurements with greater than 0.1 mag are not represented in this chart (see Table 1).

Fig. 5.— Lightcurve in 3 optical colors for SN1998bw showing the exponential decay at late times expected if the energy input is from a radioactive unstable element produced in the SN explosiont and then ejected. This is believed to be copiously produced ^{56}Ni, which decays in 6 days to ^{56}Co, which decays in 77 days to ^{56}Fe. The observed decay half life is $\sim$50 days, which is that expected for ^{56}Co as modified by the effect of expansion of the shell, and leakage of gamma rays. Fig. 1 of McKenzie & Schaefer, 1999, PASP, 111, 964.

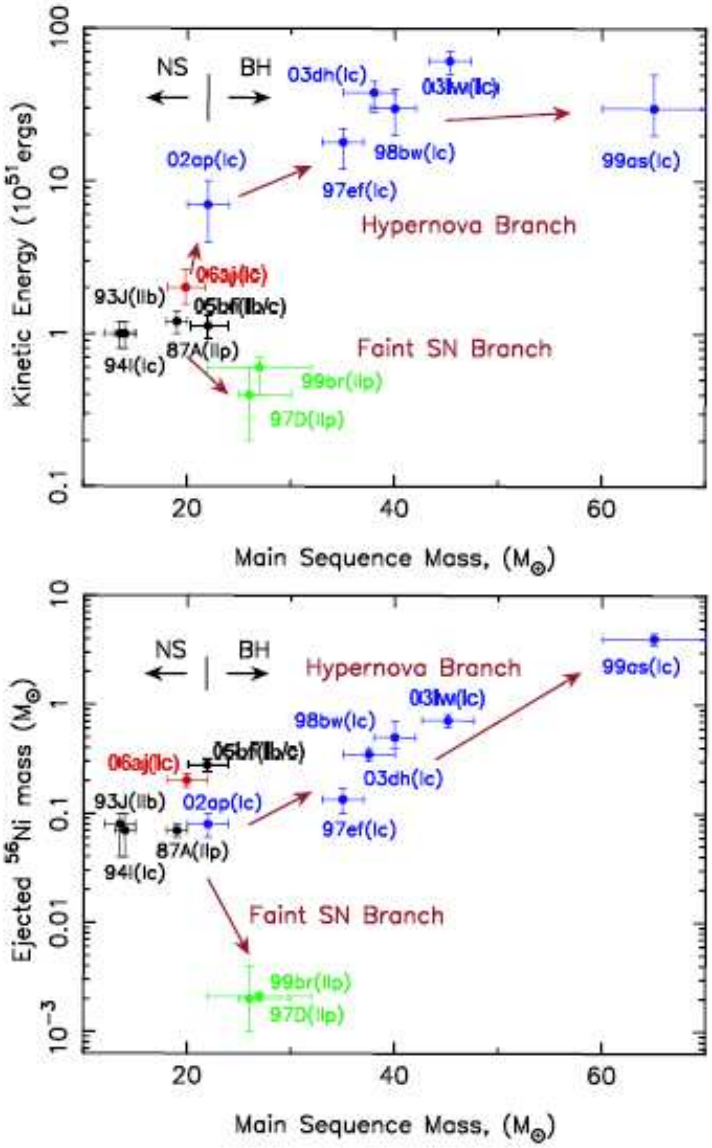

Fig. 1. The explosion energy and the ejected ^{56}Ni mass as a function of the main sequence mass of the progenitors for several supernovae/hypernovae.

Fig. 6.— Fig. 1 from Nomoto et al (2006)

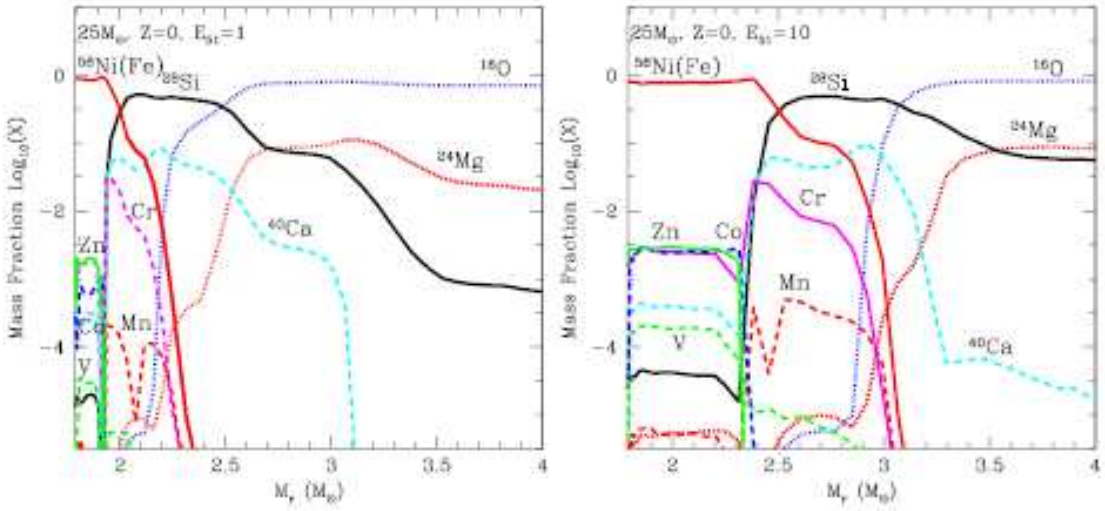

Fig. 2. Abundance distribution against the enclosed mass M_r after the explosion of Pop III 25 $M_\odot$ stars with $E_{51} = 1$ (top) and $E_{51} = 10$ (bottom) (109).

Fig. 7.— Fig. 2 from Nomoto et al (2006)

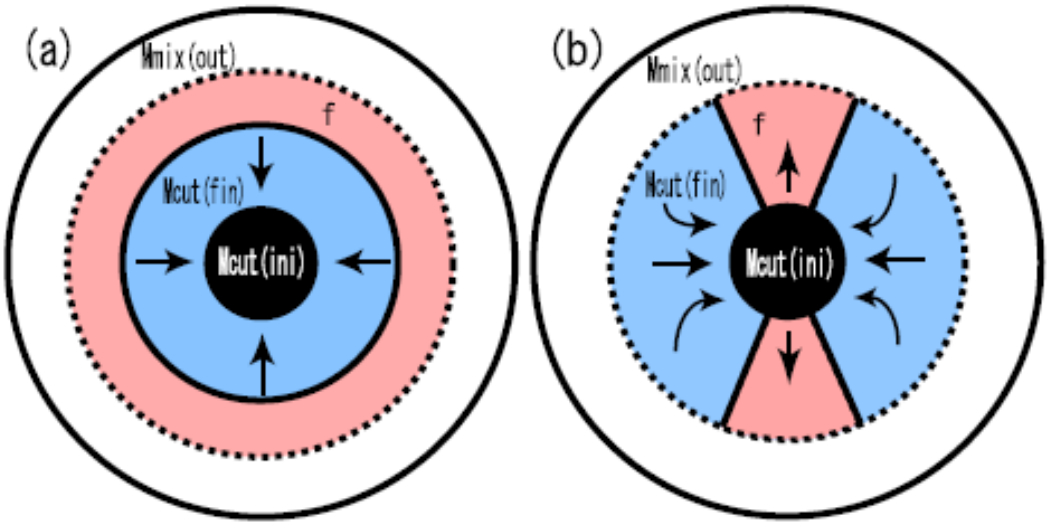

Fig. 3. The illustration of the mixing-fallback model. The central black region is the initial mass cut, that is, inside the inner boundary of the mixing region, $M_{\rm cut}$(ini). The mixing region is enclosed with the dotted line at $M_{\rm mix}$(out). A fraction f of the materials in the mixing region is ejected into the interstellar space. The rest materials, locating in the gray region inside of $M_{\rm cut}$(fin), undergo fallback onto the central remnant. (a) 1-dimensional picture: The materials mixed up to a given radius, and a part of the materials are ejected. (b) 2-dimensional picture: While all materials in the outer region above $M_{\rm mix}$(out) are ejected, the materials in the mixing region may be ejected only along the jet-axis. In the jet-like explosion, the ejection factor f depends on the jet-parameters (e.g., an opening angle and an energy injection rate).

Fig. 8.— Fig. 3 from Nomoto et al (2006)

Table 1
Stabilities of Pop III and Pop I massive stars: ◯ and × indicate that the star is stable and unstable, respectively. The e-folding time for the fundamental mode is shown after × in units of 10^4yr ([81]).

$M(M_\odot)$	80	100	120	150	180	300
Pop III	◯	◯	◯	× (9.03)	× (4.83)	× (2.15)
Pop I	◯	× (7.02)	× (2.35)	× (1.43)	× (1.21)	× (1.71)

Fig. 9.— Table 1 from Nomoto et al (2006)

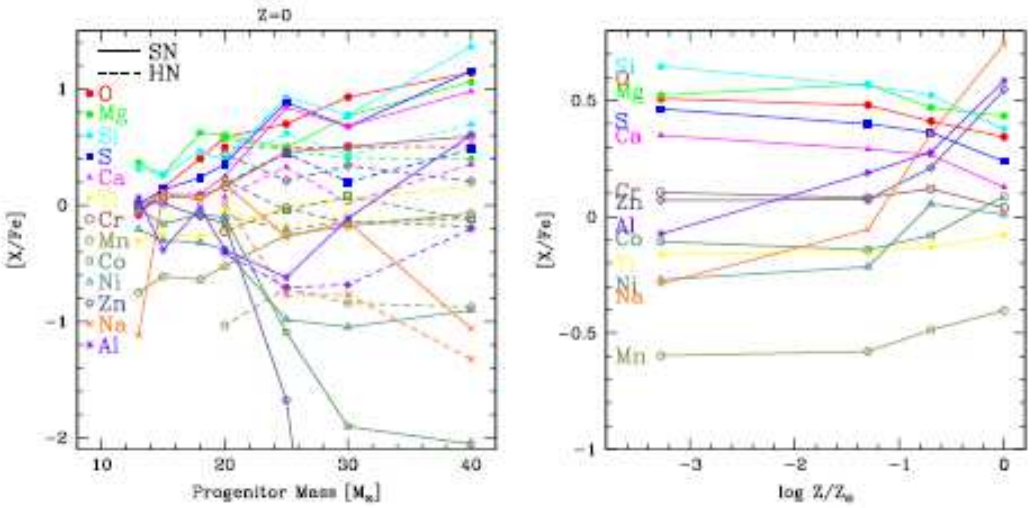

Fig. 11. (left:) Relative abundance ratios as a function of progenitor mass with $Z = 0$. The solid and dashed lines show normal SNe II with $E_{51} = 1$ and HNe. (right:) The IMF weighted abundance ratios as a function of metallicity of progenitors, where the HN fraction $\epsilon_{\rm HN} = 0.5$ is adopted. Results for $Z = 0$ are plotted at $\log Z/Z_\odot = -4$.

Fig. 10.— Fig. 11 from Nomoto et al (2006)

Table 2
The yields of individual SN models.

$Z = 0$							
M	13	15	18	20	25	30	40
E	1	1	1	1	1	1	1
$M_{\rm cut}$	1.57	1.48	1.65	1.66	1.92	2.07	2.89
p	6.59E+00	7.58E+00	8.43E+00	8.77E+00	1.06E+01	1.17E+01	1.40E+01
d	1.49E−16	1.69E−16	1.28E−16	8.66E−17	2.02E−16	1.34E−16	3.46E−16
^{3}He	4.12E−05	4.09E−05	3.33E−05	4.76E−05	2.11E−04	2.06E−04	2.56E−05
^{4}He	4.01E+00	4.40E+00	5.42E+00	5.94E+00	8.03E+00	9.52E+00	1.19E+01
^{6}Li	3.65E−23	1.11E−22	4.37E−23	3.65E−21	2.69E−21	1.13E−22	7.54E−22
^{7}Li	2.17E−10	2.94E−10	7.34E−11	2.79E−10	5.68E−09	2.36E−08	3.76E−11
^{9}Be	1.77E−20	3.22E−22	1.05E−22	4.49E−23	1.24E−17	1.26E−20	5.33E−20
^{10}B	2.92E−21	8.30E−20	3.92E−21	1.57E−19	2.87E−18	5.18E−20	2.37E−17
^{11}B	2.94E−16	3.30E−16	7.14E−16	6.54E−17	9.46E−16	3.27E−15	3.07E−14
^{12}C	7.41E−02	1.72E−01	2.18E−01	2.11E−01	2.94E−01	3.37E−01	4.29E−01
^{13}C	8.39E−08	6.21E−08	2.63E−09	1.14E−08	1.47E−08	1.02E−08	3.21E−09
^{14}N	1.83E−03	1.86E−03	1.89E−04	5.42E−05	5.91E−04	1.64E−06	5.89E−07
^{15}N	6.38E−08	6.86E−08	2.40E−08	1.13E−08	1.17E−07	1.67E−08	6.29E−07
^{16}O	4.50E−01	7.73E−01	1.38E+00	2.11E+00	2.79E+00	4.81E+00	8.38E+00
^{17}O	1.69E−06	1.57E−06	2.79E−07	6.83E−08	1.49E−06	1.88E−08	1.42E−09
^{18}O	5.79E−08	4.89E−06	4.63E−06	2.52E−08	6.75E−07	2.06E−09	2.13E−07
^{19}F	1.17E−10	1.97E−09	7.91E−09	1.62E−09	1.71E−09	8.94E−10	2.38E−10
^{20}Ne	1.53E−02	3.27E−01	4.94E−01	9.12E−01	5.33E−01	8.51E−01	3.07E−01
^{21}Ne	5.42E−07	3.76E−05	9.12E−05	4.30E−05	1.33E−05	5.51E−05	1.08E−05
^{22}Ne	1.98E−07	1.61E−05	2.57E−05	6.92E−05	2.02E−05	8.57E−05	6.75E−06
^{23}Na	1.44E−04	2.45E−03	2.08E−03	2.90E−03	1.03E−03	1.42E−03	1.84E−04
^{24}Mg	8.62E−02	6.82E−02	1.57E−01	1.50E−01	1.20E−01	2.26E−01	4.78E−01
^{25}Mg	1.56E−04	2.98E−04	5.83E−04	1.16E−04	3.97E−05	2.44E−04	4.28E−04
^{26}Mg	7.07E−05	3.98E−04	8.73E−04	2.38E−04	5.01E−05	1.29E−04	1.25E−04

Fig. 11.— The beginning of a yield table (Table 2) from Nomoto et al (2006)

3.1. Pair Instability SN Yields

Extremely massive stars with initial $M > 140M_{\odot}$, if such exist, have oxygen cores which exceed $M_c = 50M_{\odot}$. These can reach very high temperatures at relatively low densities. Conversion of energetic photons into electron-positron pairs occurs prior to oxygen ignition. The gas is largely radiation pressure supported, so when this happens and the radiation pressure drops abruptly, a violent contraction triggers a catastrophic nuclear explosion whose energy unbinds the star completely, leaving no remnant at all. Until very recently, there has been no detected PISN in all of the very many active and past SN searches. Thus it was believed that if PISN acutally occur, they would be confined to the early Universe, where 0 metallicity would permit such high mass stars to be formed and to evolve.

Such stars, if present, would be tremendously important in chemical evolution because of the very large amount of ejected material. Their nucleosynthesis, first worked out in detail in Heger & Woosley (2002, ApJ, 567, 532) (look for their cases where $140 < M/M_{\odot} < 260$), is characterized by an extremely large odd-even effect, far larger than that observed in any known Galactic star, suggesting that even in the early Universe, PISN were rare or absent. More than $50M_{\odot}$ of ^{56}Ni can be formed during the collapse, but no elements beyond Zn are produced as there are no neutron capture processes. An interesting alternative view is presented by Karlsson, Johnson & Bromm (2008, ApJ, 679, 6) who claim to be able to hide PISN ejecta in a clever way.

The first detection of a PISN was recently claimed by Gal-Yam, Mazzali, Ofek et al (2009, Nature, 462, 624), SN 2007bi, whose host is a dwarf galaxy with mass about 1% that of the Milky Way, presumably of low mean metallicity. They claim that based on the high extremely luminosity of this SN at peak, and the slow rise time to peak, that the kinetic energy released was $\sim 10^{53}$ ergs, the exploding core mass is likely to be $\sim 100M_{\odot}$, and that

more than $3M_{\odot}$ of ^{56}Ni was synthesized. They thus infer that SN 2007bi must have been a PISN.

Somewhat lower mass stars may become pulsational pair instability SN, suggested for stars in the mass range 95 to $130M_{\odot}$ by Woosley, Blinnikov & Heger (2007, Nature, 450, 390). The scenario proceeds as above, but in this case, the energy released by the explosive burning is inadequate to unbind the star, which ejects many solar masses of surface material in a series of giant pulses.

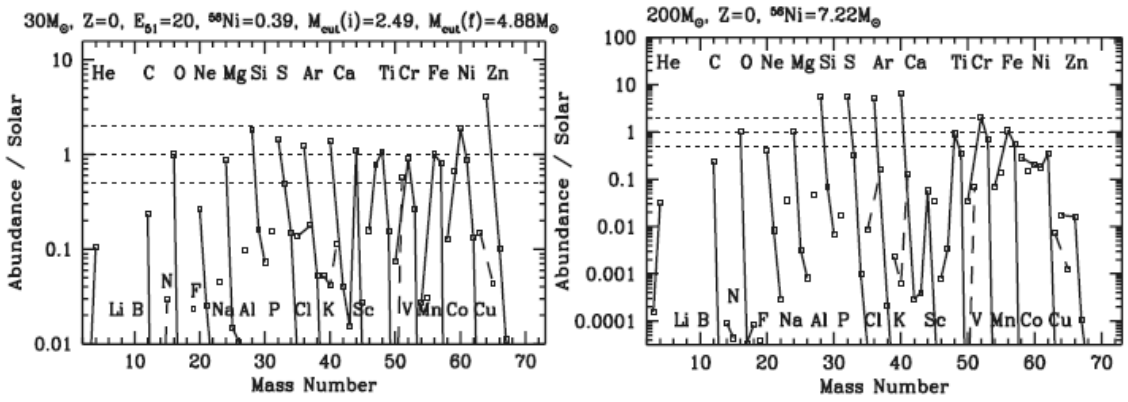

Figure 2: The abundance pattern of a hypernova (left) and a PISN model (right panel), normalize to the solar abundance. For PISNe with initial masses $M \simeq 140 - 300 M_{\odot}$ [Zn/Fe] is small, so that the abundance features of very metal-poor halo stars cannot be explained by these SNe.

Fig. 12.— Fig. 2 from Umeda & Nomoto, 2002, Conference proceeding, Astro-ph/0205365). Note the different vertical scale in the two panels. The odd-even effect is about 100 times larger in the PISN than in the hypernova.

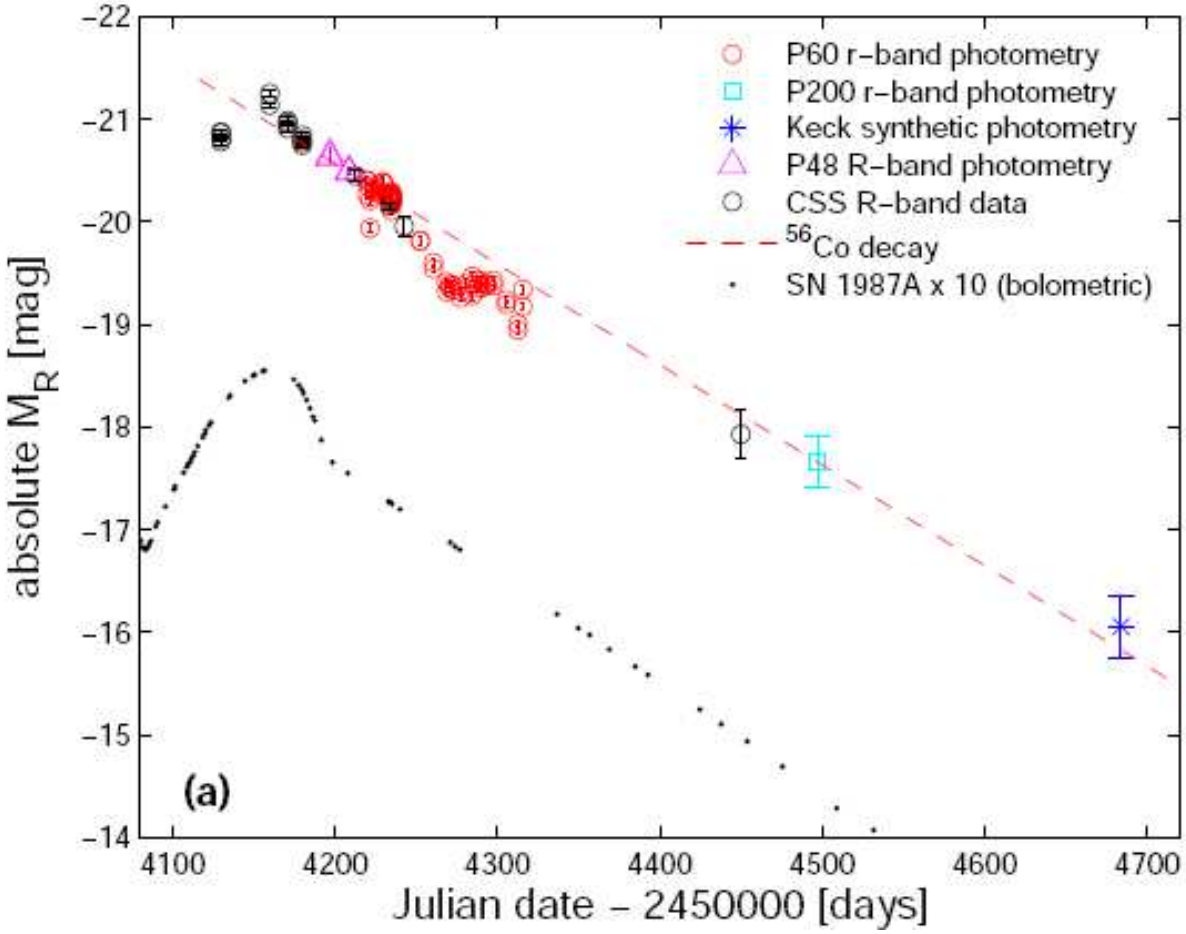

Fig. 13.— The light curve for SN 2007bi, the PISN candidate identified by Gal-Yam, Mazzali, Ofek et al (2009, Nature, 462, 624). The light curve follows the ^{56}Co decay rate. The lower light curve is that of SN 1987A in the LMC multiplied by a factor of 10 in luminosity.

4. Asymptotic Giant Branch Stars

AGB stars represent the last nuclear burning phase for stars with initial masses from about 0.8 to $8M_{\odot}$. AGB nucleosynthesis was first discussed in detail by Renzini & Voli (1981, A&A, 94, 175), as part of an effort to explain the luminosity and frequency of carbon stars in the LMC and in the SMC. Such stars are believed to contribute significantly to the light elements, and also be the dominant site for production of the heavy *s*-process elements. The latter requires some contortions, mixing fresh unburned H into regions in which H has already been burned into He, to produce ^{13}C, which then produces neutrons to operate the *s*-process. This is believed to happen as a result of a series of He shell flashes at intervals of $\sim 10^4$ yr in a star burning H and He in separate narrow shells. See Busso, Gallino & Wasserburg (1999, ARA&A, 37, 239) for a detailed discussion of the operation of the *s*-process in AGB stars.

The *s*-process is metallicity dependent in the sense that Fe-peak nuclei are needed as seeds for producing the rare heavier nuclei. Then, since these stars do not explode, but rather lose mass by surface winds, the processed material from the center must be mixed upward in the star close enough to the surface that convection zones can bring the material to the surface, where it can be spread into the ISM by the stellar wind. Eventually, after between 15 and 100 flashes, the star becomes pulsationally unstable, and the mass loss rate becomes very high, terminating the AGB phase.

Only species that can be produced by H and He burning are produced in AGB stars. AGB stars, through internal processing, burn O into Na, Mg into Al, and carbon into nitrogen. They produce the rare isotopes of Mg (^{25,26}Mg).

The key species for which AGB stars make important contributions are C, N, O, ^{19}F, ^{23}Na, ^{31}P (the only stable isotopes of the odd atomic number elements F, Na and P) and specific isotopes of abundant elements formed in low abundance in standard stellar

nucleosynthesis, including ^{25,26}Mg (most Mg is ^{24}Mg), and ^{30}Si (only 3% of Solar Si, Si is 92% ^{28}Si in the Sun), as well as the heavy *s*-process neutron capture elements.

Although AGB yields are low, and the amount of material per AGB star returned to the ISM is not large, there are many more AGB stars in a stellar population with a typical IMF than there are SN of any kind. Thus the cumulative effect on the chemical inventory of a galaxy from AGB stars can be large for specific species.

Amanada Karakas and John Lattanzio have been working on this issue. Karakas (2010, MNRAS, arXiv:0912.2142) gives her latest tabulation of yields, updating those given by Karakas & Lattanzio (2007). The new yields are given as electronic tables in their recent paper; their earlier yields from their 2007 study can be found online at www.mso.anu.edu.au/∼akaraks/stellar_yields. Calculation of these yields requires a deep understanding of stellar evolution, and mixing, and many poorly known parameters must be specified. Among these is the mass loss rate that is assumed.

The yields from Karakas (2010) are given for a set of 15 values of the stellar mass from 1 to 6.5$M_{\odot}$, and for metallicity from 1/200 Solar to the Solar value (4 metallicities) as online tables, where they define the yield for species i as

$$M_i \;=\; \int_0^{\tau} [X_i - X_0(i)] \frac{dM}{dt} dt,$$

M_i is in solar masses, dM/dt is the current mass loss rate, X_i and $X_0(i)$ are the current and initial mass fraction of species i, and τ is the total lifetime of the stellar model. If the yield is negative, the species is destroyed, if the species is produced, the yield is postitive.

The head of one such table is given below as an example. The last column in the table is the production factor $f = log[X_i/X_0(i)]$.

Other recent calculations of AGB star yields include those of Stancliffe & Jeffery (2007,

MNRAS, 375, 1280) and Ventura & D'Antona (2009, A&A, 499, 835). The differences among them appear to be due to differences in the stellar models, the treatment of convection, etc.

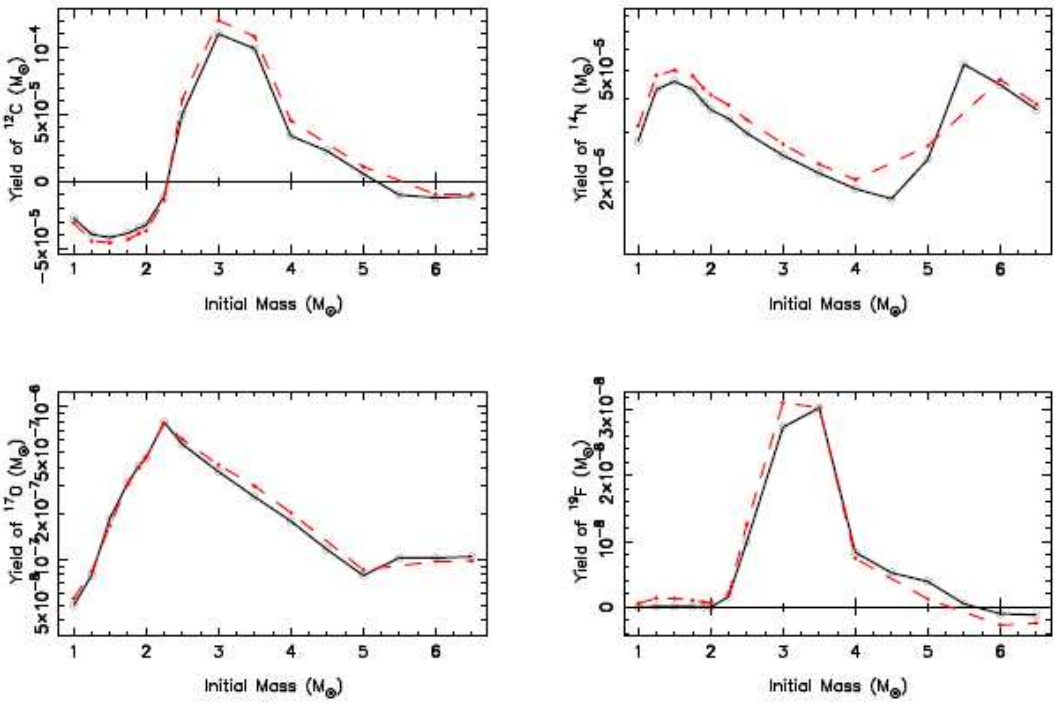

Figure 2. Weighted yields of ^{12}C, ^{14}N, ^{17}O, and ^{19}F as a function of the initial mass for the $Z = 0.02$ models. The solid line and open circles show results for the updated yields; the dashed line and filled circles show results from Karakas & Lattanzio (2007).

Fig. 14.— Fig. 2 from Karakas (2010).

Table 4. Yields for selected isotopes from the $3M_{\odot}$ models. The first line shows the yield from the model with no PMZ, the second line the yield from the PMZ model, and the third line the percentage difference between the yields.

Z	^{19}F	^{22}Ne	^{23}Na	^{25}Mg	^{26}Mg	^{30}Si	^{31}P	^{60}Fe
0.02	3.4087(−6)	1.8092(−3)	5.0942(−5)	1.0767(−5)	1.3568(−5)	7.7026(−7)	8.0023(−8)	9.5257(−9)
	4.1292(−6)	3.4512(−3)	9.2811(−5)	2.1733(−5)	2.5835(−5)	3.1746(−6)	1.6082(−6)	2.2711(−8)
	21.1%	90.8%	82.2%	102%	90.4%	312%	1910%	138%
0.008	1.1481(−5)	4.2290(−3)	7.3897(−5)	6.7804(−5)	7.3233(−5)	2.5349(−6)	2.7079(−7)	3.4270(−7)
	1.3700(−5)	7.5472(−3)	1.6357(−4)	1.0954(−4)	1.3010(−4)	3.1024(−6)	2.1346(−6)	4.0355(−7)
	19.3%	78.5%	121%	61.6%	77.6%	22.4%	688%	17.8%
0.004	1.1311(−5)	3.4789(−3)	4.3768(−5)	1.0715(−4)	1.4453(−4)	2.9138(−6)	4.1899(−7)	1.4891(−6)
	1.4083(−5)	6.9083(−3)	1.0657(−4)	1.8292(−4)	2.7583(−4)	3.8189(−6)	1.9773(−6)	1.7557(−6)
	24.5%	98.6%	143%	70.7%	90.8%	31.1%	372%	18.0%

Fig. 15.— Table 4 from Karakas (2010). These are for a $3M_{\odot}$ model for three different metallicities. For several specific isotopes produced in each model in the grid, the yield with no PMZ, then the yield assuming their standard PMZ, then the percentage difference between yields for these two assumptions is tabulated. PMZ = partial mixing zone, part of the detailed modeling of the convection zones in the AGB star.

Table 4. Yields for selected isotopes from the $3M_{\odot}$ models. The first line shows the yield from the model with no PMZ, the second line the yield from the PMZ model, and the third line the percentage difference between the yields.

Z	^{19}F	^{22}Ne	^{23}Na	^{25}Mg	^{26}Mg	^{30}Si	^{31}P	^{60}Fe
0.02	3.4087(−6)	1.8092(−3)	5.0942(−5)	1.0767(−5)	1.3568(−5)	7.7026(−7)	8.0023(−8)	9.5257(−9)
	4.1292(−6)	3.4512(−3)	9.2811(−5)	2.1733(−5)	2.5835(−5)	3.1746(−6)	1.6082(−6)	2.2711(−8)
	21.1%	90.8%	82.2%	102%	90.4%	312%	1910%	138%
0.008	1.1481(−5)	4.2290(−3)	7.3897(−5)	6.7804(−5)	7.3233(−5)	2.5349(−6)	2.7079(−7)	3.4270(−7)
	1.3700(−5)	7.5472(−3)	1.6357(−4)	1.0954(−4)	1.3010(−4)	3.1024(−6)	2.1346(−6)	4.0355(−7)
	19.3%	78.5%	121%	61.6%	77.6%	22.4%	688%	17.8%
0.004	1.1311(−5)	3.4789(−3)	4.3768(−5)	1.0715(−4)	1.4453(−4)	2.9138(−6)	4.1899(−7)	1.4891(−6)
	1.4083(−5)	6.9083(−3)	1.0657(−4)	1.8292(−4)	2.7583(−4)	3.8189(−6)	1.9773(−6)	1.7557(−6)
	24.5%	98.6%	143%	70.7%	90.8%	31.1%	372%	18.0%

Fig. 16.— The begining of Table A6 from Karakas (2010), a detailed yield table for a star with initial mass $3M_{\odot}$ and the Solar metallicity.

Table 2. Chemical yields of intermediate-mass models

$M/M_\odot$	Y	[C/Fe]	[N/Fe]	[O/Fe]	[Na/Fe]	[Mg/Fe]	[Al/Fe]	R(CNO)	C/O	$^{25}Mg/^{24}Mg$	$^{26}Mg/^{24}Mg$
					$Z = 10^{-4}$						
3.0	0.259	1.78	3.17	1.54	2.24	1.03	1.46	72.68	0.65	2.33	0.80
3.5	0.281	1.43	3.11	1.32	2.19	0.90	1.30	57.03	0.48	1.65	0.58
4.0	0.305	1.12	2.97	1.08	1.90	0.71	1.16	39.23	0.41	1.87	0.50
4.5	0.321	1.07	2.80	0.83	1.51	0.54	1.19	26.77	0.65	7.23	1.35
5.0	0.333	0.72	2.60	0.45	0.94	0.24	1.26	14.68	0.74	16.90	2.39
5.5	0.343	0.33	2.14	-0.07	0.28	-0.45	0.48	5.49	0.93	9.94	0.74
6.0	0.351	-0.58	1.40	-1.43	-0.20	-0.53	0.20	0.95	2.62	17.02	0.42
					$Z = 2 \times 10^{-4}$						
3.0	0.258	1.29	2.79	1.04	1.93	0.71	0.88	28.04	0.66	0.71	0.30
3.5	0.279	1.12	2.77	0.96	1.88	0.72	0.99	26.07	0.54	0.85	0.31
4.0	0.300	0.82	2.64	0.77	1.61	0.58	0.93	18.74	0.47	1.24	0.30
4.5	0.320	0.73	2.46	0.51	1.17	0.43	1.10	12.36	0.65	6.40	1.00
5.0	0.315	0.45	2.26	0.19	0.70	0.20	1.23	7.51	0.68	14.47	1.92
5.5	0.343	0.12	1.93	-0.30	0.22	-0.18	0.94	3.43	0.89	16.57	0.91
6.0	0.350	-0.50	1.48	-1.02	-0.10	-0.21	0.61	1.16	0.99	27.95	0.72
6.3	0.354	-0.60	1.42	-1.05	-0.14	-0.02	0.69	1.00	0.97	48.11	1.02

Fig. 17.— The begining of Table 2 from Ventura & D'Antona (2009), a detailed yield table. Note the different definition of the tabulated quantity from those tabulated by Karakas.

5. Novae

Nova explosions occur when a critical hydrogen rich envelope is reached on the white dwarf component of the nova binary, by accretion from its low mass companion. There is a thermonuclear runaway in the H rich envelope of a CO white dwarf. Novae occur fairly frequently, perhaps 20 per year in our Galaxy. Unlike in a SNIa, the nova star is not disrupted, it continues as a white dwarf in a binary system. Presumably, assuming mass transfer continues, the nove explosion will recur.

There is a class called recurrent novae where the recurrence timescale is short enough, perhaps 20 to 50 years, that multiple nova outbursts have been recorded for a particular star. Schaefer, Pagnotta, Xiao et al (2010, arXiv:1004.2842) discuss the recurrent nova U Sco, for which the tenth recorded eruption was observed earlier this year. It has outbursts at intervals of about 10 years. They estimate the total mass accreted between eruptions by integrating the energy emitted over that period from the light curve, and show that is is a constant, which suggests a white dwarf with mass close to the Chandrasekhar limit, and a high accretion rate.

Nova explosions are much less energetic than a SN; the ejection velocities are much lower ($\sim$ 1000 km/sec), the ejected mass is low ($\sim 10^{-4} M_\odot$), etc. Since nova outbursts are often detected within our galaxy, we can watch the light curves as the ejecta cool, and actually see dust formation in the ejecta in some cases.

Early calculations of the nuclear reactions that are expected to occur in novae were given by Starrfield, Truran, Sparks & Arnould (1978, ApJ, 222, 600). A more recent analysis of nova nucleosynthesis yields can be found in Gehrz, Truran, Williams & Starrfield (1998, PASP, 110, 743). In particular, if the acreting donor star loses most of its envelope, the material transfered can include partially burned H, in particular include ^{3}He, and thus novae can produce Li. Nova ejecta often contain large amounts of N and O, and novae also

produce the rare CNO isotopes.

Nova abundances are inferred from the emisison line spectra of their ejecta. Some novae show large excesses of Ne. (See, e.g. Gehrz et al (2007, ApJ, 672, 1167, *The Neon Abundance in the Ejecta of QU Vul From Late-Epoch IR Spectra*). It is believed that the neon is not produced in the explosion itself, but rather results from mixing of material in the CO core of the nova progenitor (the white dwarf itself) (which includes a lot of Ne) with the accreted envelope. Jose, Hernanz, Garcia-Berro & Pons (2003, ApJL, 597, L41) carry out some relevant modeling which supports this conjecture. This implies that there is a minimum mass at which elements beyond CNO should be expected to be enhanced in the nova ejecta, which is $M_i \sim 9.3\ M_\odot$.

More on novae can be found in the lecture notes on *The Physics of Classical Novae*, 1990, Springer Verlag, Lecture Notes in Physics, 369, 138.

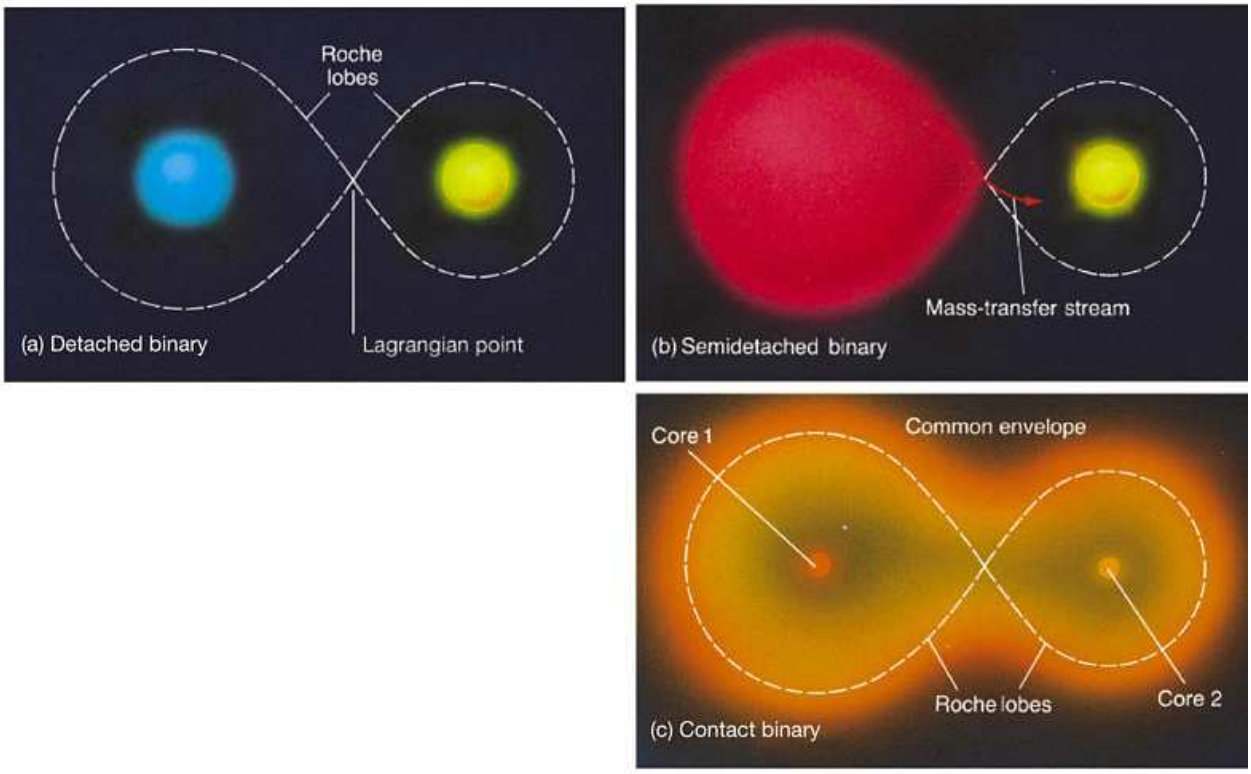

Fig. 18.— The Roche lobe and mass transfer in binary systems.

Table 9. Mass-fraction abundances of measured elements in Nova Cyg 2006 and, for reference, in the Sun.

	mass-fractions	
	NCyg	*Sun*
X	0.427	0.704
Y	0.185	0.279
Z	0.388	0.017
N	0.219	0.001
O	0.163	0.008
Ne	0.0013	0.0017
Ar	0.00008	0.00011
Fe	0.00096	0.00126

Fig. 19.— Huge enhancements of N and O, by factors of about 200 for N and 20 for O, in the ejecta of Nova Cyg 2006, with Ne, Ar, and Fe normal, and H and He depleted compared to Solar ratios. These were found by looking at emission lines arising from the ejected material. (Table 9 of Munari, Siviero, Henden et al, 2008, A&A, 492, 145)